Journal of Radiation Research, Vol. 58, No. 3, 2017, pp. 386–396
doi: 10.1093/jrr/rrw104
Advance Access Publication: 3 November 2016

Feasibility study of a non-invasive eye fixation and monitoring device using a right-angle prism mirror for intensity-modulated radiotherapy for choroidal melanoma

Toshihiko Inoue[1,3], Norihisa Masai[1*], Hiroya Shiomi[1], Ryoong-Jin Oh[1], Kenji Uemoto[1] and Noriyasu Hashida[2]

[1]Miyakojima IGRT Clinic, 1-16-22, Miyakojimahondori, Miyakojima-ku, 534-0021, Japan
[2]Department of Ophthalmology, Osaka University Graduate School of Medicine, 2-2 Yamadaoka, Suita, Osaka 565-0871, Japan
[3]Present address: Ashiya Radiotherapy Clinic Nozomi, 3-84 Yoko-cho, Ashiya, 659-0034, Japan.
*Corresponding author. Miyakojima IGRT Clinic, 1-16-22, Miyakojimahondori, Miyakojima-ku, Osaka, 534-0021, Japan. Tel/Fax +81-6-6923-3501; Email:nmasai@osaka-igrt.or.jp
Received February 4, 2016; Revised June 5, 2016; Accepted September 30, 2016

ABSTRACT

We aimed to describe the feasibility and efficacy of a novel non-invasive fixation and monitoring (F-M) device for the eyeballs (which uses a right-angle prism mirror as the optic axis guide) in three consecutive patients with choroidal melanoma who were treated with intensity-modulated radiotherapy (IMRT). The device consists of an immobilization shell, a right-angle prism mirror, a high magnification optical zoom video camera, a guide lamp, a digital voice recorder, a personal computer, and a National Television System Committee standard analog video cable. Using the right-angle prism mirror, the antero–posterior axis was determined coincident with the optic axis connecting the centers of the cornea and pupil. The axis was then connected to the guide light and video camera installed on the couch top on the distal side. Repositioning accuracy improved using this method. Furthermore, the positional error of the lens was markedly reduced from ±1.16, ±1.68 and ±1.11 mm to ±0.23, ±0.58 and ±0.26 mm in the horizontal direction, and from ±1.50, ±1.03 and ±0.48 mm to ±0.29, ±0.30 and ±0.24 mm in the vertical direction (Patient #1, #2 and #3, respectively). Accordingly, the F-M device method decreased the planning target volume size and improved the dose–volume histogram parameters of the organ-at-risk via IMRT inverse planning. Importantly, the treatment method was well tolerated.

KEYWORDS: feasibility study, eye fixation and monitoring device, optic axis guide, intensity-modulated radiotherapy, choroidal melanoma

INTRODUCTION

Choroidal melanoma is a rare type of cancer with an annual crude incidence rate of 0.03/100 000 population in Japan [1], which amounts to ~40 patients per year. The treatment strategy depends on the tumor size: large tumors are treated with enucleation, medium-sized tumors with proton beam irradiation, and small tumors with brachytherapy [2–4]. Recently, carbon ion–based treatment has been challenging for large tumors in Japan [5, 6], and stereotactic radiotherapy (SRT) has been challenging for small to medium tumors in Western countries [3]. They have demonstrated efficacy for the treatment of melanoma, however some of issues have been remaining such as anterior segment complication and invasive eye immobilization. Curative treatment for choroidal melanoma achieved with external beam radiotherapy mandatorily involves not only fixation of the patient, but also immobilization and monitoring of the affected eye's motion [7]. Owing to the need for a special fixation system, various methods have been established for administering particle beam therapy and SRT for choroidal melanoma [8–15]. We developed a non-invasive fixation and monitoring (F-M) device for the eyeballs using a right-angle prism mirror,

wherein the gazing direction can be adjusted to the optic axis. This method enables immobilization of the affected eye in the correct position during the planning computed tomography (CT) scan and during treatment delivery. We used intensity-modulated radiotherapy (IMRT) to obtain dose homogeneity in the target volume. This permits a free beam arrangement to avoid irradiating the organ at risk (OAR). In addition, it is possible to constrain the dose for the OAR. In this study, we assessed the feasibility and efficacy of this non-invasive F-M device for the eyeballs.

PATIENTS AND METHODS

Patients

From March 2013 to December 2014, three patients (two males, one female) with choroidal melanoma were consecutively treated with IMRT at an image-guided radiation therapy clinic. Patient and tumor characteristics are shown in Table 1. The patients underwent ophthalmological examination and were diagnosed with choroidal melanoma at the University Hospital. In all cases, a dome-shaped tumor at the posterior arcade of the retina was observed. The median tumor length and thickness was 11.8 mm (range, 10.0–12.8 mm) and 5.7 mm (range, 3.3–6.6 mm), respectively. The median tumor volume was 315 mm^3 (range, 92–428 mm^3). These volumes were evaluated using optical coherence tomography (OCT), and differed slightly in numerical values in comparison with the volume of the CT-based treatment planning. The median distances from the fovea and disc were 5.8 mm (range, 5.3–13.3 mm) and 9.6 mm (range, 7.1–11.4 mm), respectively.

We obtained written informed consent from each patient for treatment using this method. The plenary meeting approved the study protocol, including the chart review.

Equipment

We used a 6-MV X-ray Novalis™ unit (BrainLAB AG, Germany). A four-slice BrightSpeed Excel™ (GE, USA) unit served as the CT-simulator, SIGNA EXCITE HDx 1.5T™ (GE, USA) as the magnetic resonance imaging (MRI)-simulator, and iPlan RT Image™ ver. 4.1.0 and iPlan RT Dose ™ ver. 4.1.2 (BrainLAB AG, Germany) units were used for the treatment planning. The HipFix™ thermoplastic positioning system (shell) and Vac-Lok™ positioning cushion (CIVCO, USA) were used to immobilize patients, and the ExacTrac™ X-ray 6D positioning system and robotic couch (BrainLAB AG, Germany) served as the image-guided radiotherapy system.

The fixation and monitoring device

We developed a non-invasive F-M device for the eyeballs with an optic axis guide. The device consists of an immobilization shell, a right-angle prism mirror, a charged coupled device (CCD) camera with a high magnification optical zoom function (GZ-E325™, JVC, Japan), a guide lamp, a digital voice recorder (ICR-PS503RM™, SANYO, Japan), a personal computer (PC), and a National Television System Committee (NTSC) standard analog video cable (Fig. 1). The NTSC analog cable connects the 30 m distance between the operation room and the treatment room. We monitored the movement of the patient's pupil by using a PC-SDVD/U2G2™ (BUFFALO, Japan), which is an NTSC standard video signal–USB flash drive adapter that can display and record images on the PC. In addition, we recorded the electronic sound that notifies the beam-on with the digital voice recorder. The sound was simultaneously recorded in the audio track of the video monitoring.

After setting up the CCD-camera to obtain the cross line on the display, the prism mirror was deposited on the immobilizing shell. On the basis of the gazing light of the guide lamp on the

Table 1. Patient and tumor characteristics

Patient #		#1	#2	#3
Age (years)		68	53	75
Sex		female	male	male
Laterality		right	left	left
TNM		T1a N0 M0	T1a N0 M0	T2a N0 M0
Stage		I	I	IIA
Tumor	Location	posterior	posterior	posterior
	Shape	dome	dome	dome
	Size (mm)	12.8 × 10.0	10.0 × 7.0	11.8 × 10.3
	Thickness (mm)	5.7	3.3	6.6
	Volume (mm^3)	428	92	315
Distance to	Fovea (mm)	5.3	5.8	13.3
	Disc (mm)	9.6	7.1	11.4
Visual acuity		0.5	0.8p	0.6

p = partial.

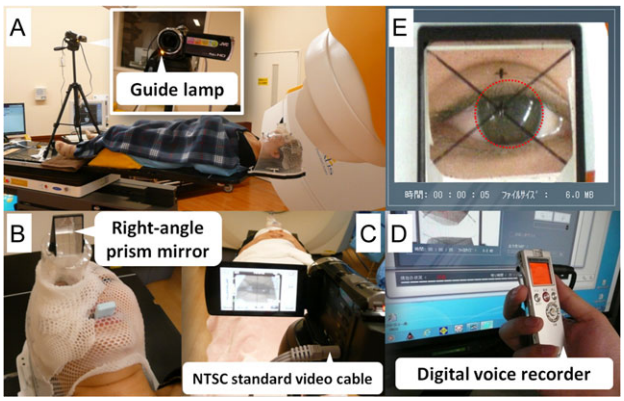

Fig. 1. Non-invasive fixation and continuous monitoring system for the eyeballs with an optic axis guide (A). The device consists of an immobilization shell, a right-angle prism mirror (B), a charged coupled device camera (A, C, E), a guide lamp (A), a digital voice recorder (D), a personal computer and a National Television System Committee (NTSC) standard analog video cable (C).

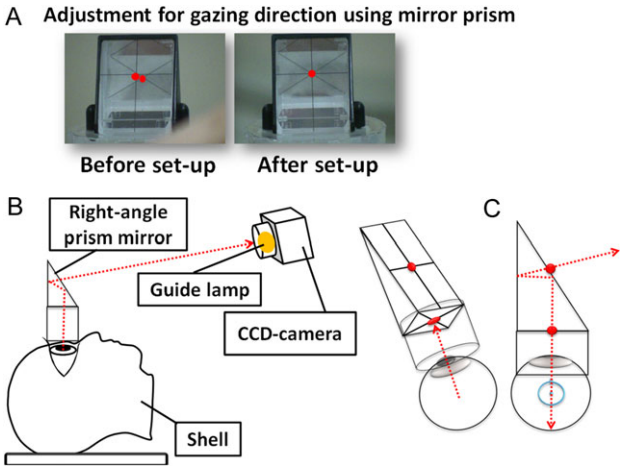

Fig. 2. Before setup, two separate red circles, which represent the visual and optic axes, are visible on the display. After complete set-up of the CCD camera to obtain the cross-line on the display (A), the prism mirror is deposited on the immobilizing shell. By means of the gazing light (B), the antero–posterior axis becomes coincident with the optic axis connecting the centers of the cornea and pupil through the right-angle prism mirror (C).

CCD-camera, the gazing direction, that is the antero–posterior axis, was chosen coincident with the optic axis connecting the cornea and pupil centers through the right-angle prism mirror (Fig. 2). The system was used in conjunction with a head shell system for immobilization and infrared tracking technology for positioning (BrainLAB AG, Germany). Accordingly, the affected eye was immobilized during the planning CT scan and the beam delivery over the five consecutive IMRT sessions. The eye's alignment during the treatment was monitored using a CCD-camera through the right-angle prism mirror, which was displayed on the monitor in the operating room.

Repositioning accuracy

During the period between the CT simulation and the first day of the treatment, we confirmed the treatment set-up error by using three CT images with the F-M device. We acquired the CT images on three consecutive days and these images were imported into the treatment planning system for bone registration. Consequently, we could verify the reproducibility of the location of the center of the gross tumor volume (GTV) by calculating the standard deviation (SD) (using the data obtained from monitoring the position of the eyeball during the CT scan using the F-M device).

Eye movement analysis

Patients underwent MRI examination of the eyeballs using the fast-imaging steady-state acquisition 2D cine-mode to determine the magnitude of the internal margin (IM). The lens motion was recorded using 60 s serial images taken at 0.5 s/frame [16]. Cine MRI images targeted the movement of the lens in the coronal plane. Motion analysis was plotted at the center of the lens in the superior-inferior (S–I) and right-left (R–L) directions, and we calculated the SD of the movement of the lens. In addition, we calculated the coordinate rotation based on the lens motion in the S–I and R–L directions, to predict the movement of the tumor located in the choroid. Furthermore, we defined the IM of the tumor using this coordinating rotation with the polar coordinate conversion formula below. G (x, y, z) represents the average GTV position, which was obtained using the three set-up CT images taken on three consecutive days before the first day of treatment. The G (x, y, z) was defined as the reference position and was assumed to be the tumor center, i.e. the average position of the eye movement with/without the F-M device (Fig. 3, upper-left).

The GTV center coordinates can be represented using the following polar coordinate conversion formula:

$$\begin{matrix} x \\ y \\ z \end{matrix} = \begin{pmatrix} r\cos\theta\cos\varphi \\ r\cos\theta\sin\varphi \\ r\sin\theta \end{pmatrix}, \quad (1)$$

where r is the radius of the eyeball. θ and φ is the angle formed by the line connecting the center of the eyeball and the GTV center (Fig. 3, lower). G' (x', y', z') is the GTV center that moves with eyeball rotational movements. Usually, the rotational motion of the sphere is a 3-axis rotation. In this study, the y-axis, i.e. rotation of the AP axis, was assumed to not occur in order to simulate the eye movement. Rotating coordinates in the x-axis and z-axis were determined using the following 3D matrix transformation equations:

$$\begin{pmatrix} x' \\ y' \\ z' \end{pmatrix}_{xz} = \begin{pmatrix} 1 & 0 & 0 \\ 0 & \cos\theta_{lens} & -\sin\theta_{lens} \\ 0 & \sin\theta_{lens} & \cos\theta_{lens} \end{pmatrix} \begin{pmatrix} \cos\varphi_{lens} & -\sin\varphi_{lens} & 0 \\ \sin\varphi_{lens} & \cos\varphi_{lens} & 0 \\ 0 & 0 & 1 \end{pmatrix} \begin{pmatrix} x \\ y \\ z \end{pmatrix}, \quad (2)$$

where θ_{lens} and φ_{lens} are the angles formed after the eyeball moves from the mean position of the lens. The θ_{lens} and φ_{lens} angles were calculated using the following formula (Fig. 3, upper-right and lower).

$$\theta_{lens} = \tan^{-1}\frac{M_{(S-I)}}{r} \quad (3)$$

$$\varphi_{lens} = \tan^{-1}\frac{M_{(R-L)}}{r} \quad (4)$$

$M_{(S-I)}$ is the lens movement in the S–I direction, and $M_{(R-L)}$ is the lens movement in the R–L direction obtained using 2D cine-mode MRI. GTV coordinates after the eyeball movement were calculated by using the conversion formulas. For the treatment planning, the IM was based on the 95% confidence interval of the SD from these movement data.

Treatment planning

The GTV was determined by combining swept-source optical coherence tomography (SS-OCT) data and CT-MRI fusion images to improve the accuracy of delineation of the GTV. We defined the GTV as the clinical target volume. The IM was based on the 95% confidence interval of the tumor motion data calculated from the eyeball movements and was defined as the internal target volume (ITV). The planning target volume (PTV) was defined as the ITV plus the set-up margin.

Dose fractionation was established as IMRT administered at 60 Gy in five fractions over 5–7 days using seven non-coplanar beams. We performed dose calculation with the Pencil-beam algorithm on the iPlan RT Dose™ ver. 4.1.2 (BrainLAB AG, Germany). Dose constraints for PTV were $D_{95} \geq 97\%$, $V_{95} \geq 97\%$, $V_{107} \leq 3\%$.

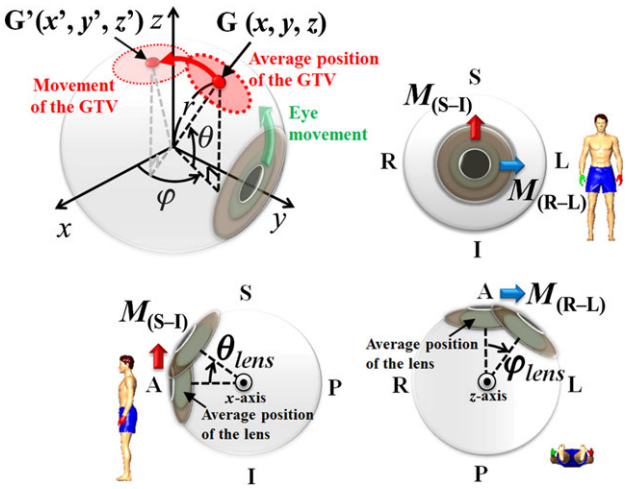

Fig. 3. G (*x*, *y*, *z*) is the center of the average gross tumor volume (GTV) position, which was obtained using the three set-up computed tomography scans. G' (*x*', *y*', *z*') is the GTV center that moves with eyeball rotation. $M_{(S-I)}$ is the lens movement in the S–I direction, and $M_{(R-L)}$ is the lens movement in the R–L direction, obtained using 2D cine-mode magnetic resonance imaging. GTV coordinates (*x*', *y*', *z*') were calculated using the conversion formulas.

RESULTS

Repositioning accuracy

The SDs of each axis of the GTV position were ±0.46, ±0.21 and ±0.29 mm (in the *x*, *y* and *z* axes) in Patient #1; ±0.10, ±0.20 and ±0.12 mm in Patient #2; and ±0.25, ±0.38 and ±0.06 mm in Patient #3. Using the F-M device, we were able to ensure that the optic axis was consistently placed in the correct position at the time of treatment preparation and at every treatment session. The GTV position was predicted by monitoring the lens. Therefore, we could easily verify the daily position of the GTV (Fig. 4).

Eye movement and internal margin

In three patients, when using the immobilization shell with closed eyes, the SDs of the lens motion were ±1.16 and ±1.50 mm (in the R–L and S–I directions, respectively) in Patient #1, ±1.68 and ±1.03 mm in Patient #2, and ±1.11 and ±0.48 mm in Patient #3. On the other hand, when using the F-M device with open eyes, the SDs of the lens motion were markedly reduced to ±0.23 and ±0.29 mm in Patient #1, ±0.58 and ±0.30 mm in Patient #2, and ±0.26 and ±0.24 mm in Patient #3 (Table 2, upper; and an example shown in Fig. 5). As a result, when using the F-M device with open eyes, the calculated tumor motions were reduced to 21%, 21% and 19% (in the *x*, *y* and *z* axis) in Patient #1; 34%, 28% and 29% in Patient #2; and 24%, 28% and 50% in Patient #3 (Table 2, middle; and an example shown in Fig. 6).

According to the calculated tumor motion, the ITVs were reduced to 39%, 62% and 50% (in Patients #1, #2 and #3, respectively) with open eyes using the F-M device with an optic axis guide.

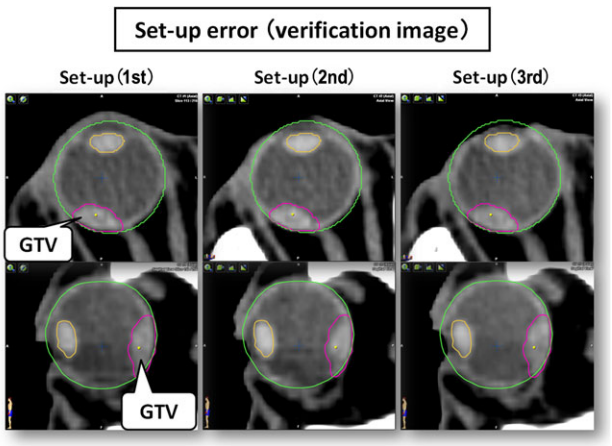

Fig. 4. Repeated computed tomography images obtained in the transverse (top) and sagittal views (bottom) verified the reproducibility of the position of the eyes using the F-M device in Patient #1. Image registration was performed not only on the bony structure with the ExacTrac system, but also on the eyeball with the optic axis guide.

Table 2. Tumor motion and volume reduction with F-M device

Patient #	#1			#2			#3		
F-M device	(−)	(+)		(−)	(+)		(−)	(+)	
Lens motion	SD (mm)		(%)	SD (mm)		(%)	SD (mm)		(%)
R-L	1.16	0.23	20	1.68	0.58	35	1.11	0.26	23
S-I	1.50	0.29	19	1.03	0.30	29	0.48	0.24	50
Tumor motion	SD (mm)		(%)	SD (mm)		(%)	SD (mm)		(%)
X	0.78	0.16	21	0.90	0.31	34	0.38	0.09	24
Y	1.02	0.21	21	0.89	0.25	28	1.17	0.33	28
Z	1.01	0.19	19	0.55	0.16	29	0.16	0.08	50
Volume	(mm^3)		(%)	(mm^3)		(%)	(mm^3)		(%)
GTV	428	428		95	95		329	329	
ITV	1367	532	39	254	158	62	753	377	50
PTV	2083	1028	41	542	395	73	1303	753	58

F-M device = fixation and monitoring device; GTV = gross tumor volume; ITV = internal target volume; PTV = planning target volume.

Finally, we defined the PTV as the ITV plus a 1.0 mm margin (Table 2, lower).

Dose–volume histogram parameters

Using the F-M device, we were able to reduce the D_{mean} to the optic nerve and retina. Point doses at the fovea and disc were markedly reduced for both Patients #1 and 3. The dose–volume histogram (DVH) parameters for the optic nerve, retina, eyeball, lens and lacrimal gland improved (Table 3). The dose for anterior segments of the orbit, such as the lens and lacrimal gland, was within acceptable limits.

Monitor units and treatment duration

All patients underwent seven-beam non-coplanar IMRT with a prescribed dose of 60 Gy in five fractions for a small PTV, of which the median volume was 753 mm^3 (range, 395–1,028 mm^3). Accordingly, the fraction dose was 12 Gy, and the median number of monitor units (MUs) required for one of seven beams requiring a fraction dose of 12 Gy was 329 (range, 310–359). However, the treatment duration necessary to deliver 12 Gy did not depend on only MUs but also on the preparation of the treatment, including patient set-up and minor adjustments for eyeball fixation. Although the median treatment duration was 28.3 min (range, 25.7–48.4 min), it varied greatly (from 27.3 to82.6 min in five consecutive treatment sessions for Patient #3, owing to treatment interruption due to a cough). The median beam-on time for delivering a prescribed dose for each of the seven beams was 41 s (range, 39–43 s); during this period, patients were required to gaze into the light continuously (Table 4).

Case presentation for Patient #1

The patient was a 68-year-old female with right choroidal melanoma, cT1aN0M0 Stage I, with a medium-sized tumor per the Collaborative Ocular Melanoma Study (COMS) classification. She reported a 2-month history of distortion and visited the Department of Ophthalmology at our hospital. Ophthalmologic examination showed decreased right visual acuity (RV) (RV = 0.5; left visual acuity (LV) = 1.0). Fundoscopy, fluorescent angiography with indocyanine green and fluorescence examination, single-photon emission CT, positron emission tomography-CT, B-scan ultrasonography, and SS-OCT findings confirmed the presence of right choroidal melanoma. After a second opinion, the patient visited an image-guided radiation therapy clinic for IMRT in March 2013.

The tumor was located at the inferior temporal arcade of the right retina. Distances from the tumor margin to the fovea and disc were estimated at 5.3 mm and 9.6 mm, respectively (Table 1). Treatment planning revealed a GTV of 12.8 × 10.0 × 5.7 mm (Fig. 7 A–C). The patient underwent curative IMRT using seven non-coplanar beams comprising 60 Gy administered in five fractions over 7 days in March 2013 (Fig. 8).

Pretreatment preparations indicated that each session would last 30 min. Although the patient complained of tiredness using the optic axis guide, she consented to this treatment. Before the treatment, she received steroid therapy to prevent early reactions. The median treatment duration was 28.3 min (range, 24.5–34.3 min) to deliver the prescribed fraction of 12 Gy (Table 4). The GTV was 428 mm^3 (Table 1).

The number of MUs required to deliver a fractional dose of 12 Gy with seven non-coplanar beams was 359 (range, 279–416). Overall treatment duration, including treatment preparation, was 28.3 min (range, 24.5–34.3 min), and the beam-on time was 43 s (range, 35–52 s) per beam; during this period, the patient was

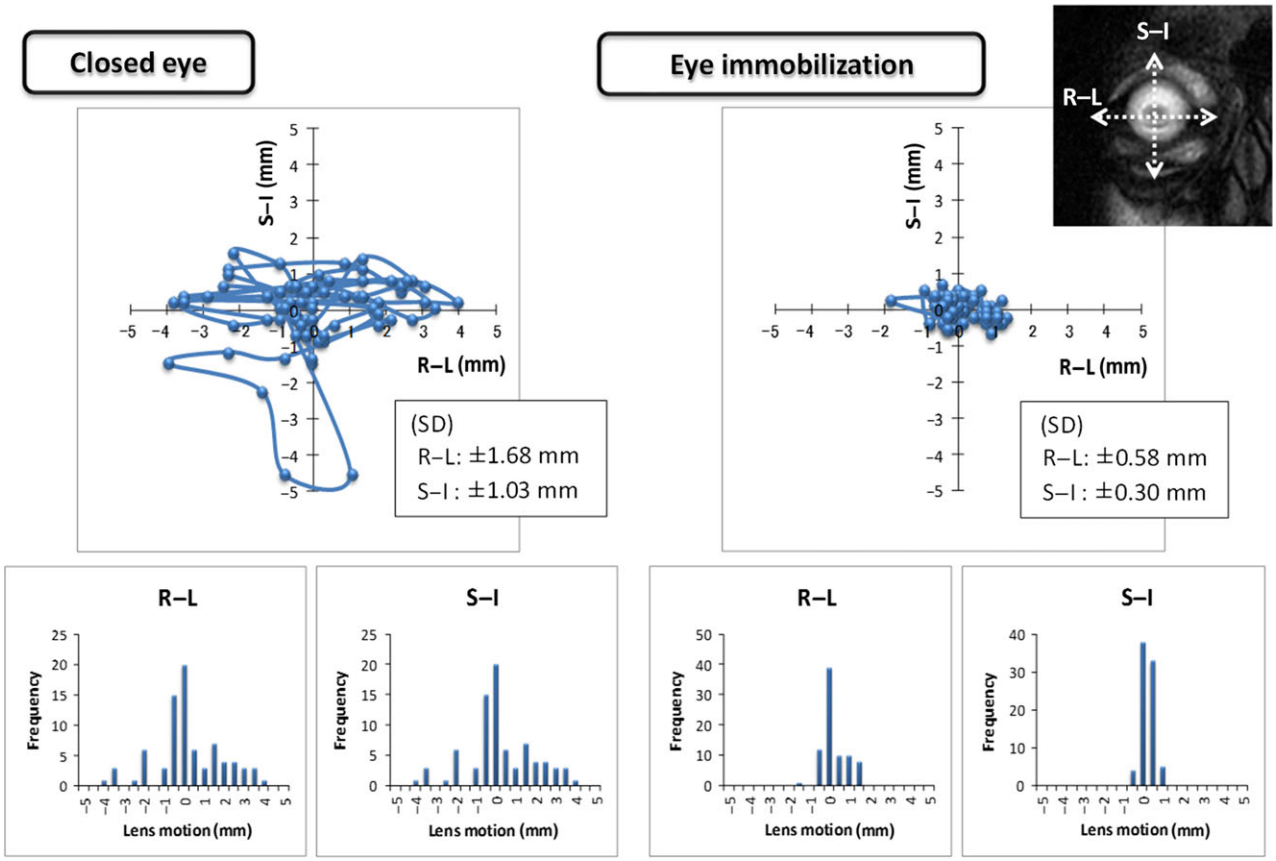

Fig. 5. Eye movement analysis performed with cine MRI images showed that the positional error of the lens was markedly reduced to ±0.58 mm in the horizontal direction (R–L) and ±0.30 mm in the vertical direction (S–I) when using the F-M device.

required to gaze at the light continuously (Table 4). The patient tolerated this F-M device well.

Two years and one month later, the patient still experienced distortion and developed a low-grade cataract without decreased visual acuity (RV = 0.7). Nonetheless, the tumor decreased in size from 428 mm^3 to 265 mm^3, which was a 38% reduction. Fundus examination revealed hard exudates encompassing the tumor (Fig. 7 D–F). The subretinal fluid was absorbed into the area of the serous detachment according to the OCT examination.

DISCUSSION

In 1980, several important studies emerged that provided evidence for the use of radiotherapy for ocular melanoma [17]. Targeted therapy using ^{125}Iodine ophthalmic plaque, proton beam, and helium ion therapy proved effective for eye melanoma [18–20]. A few years later, outcomes of the gamma knife approach were reported [21]. These treatments delivered high fractional doses and large amounts of the total dose that were biologically effective on the uveal melanoma lesion [22]. Currently, radiotherapy is the first treatment of choice for small- and medium-sized uveal melanomas [2–4, 6]. For large tumors, carbon ion therapy has proved challenging in the National Institute for Radiological Science in Chiba [5, 6]. Regarding proton beam therapy, although excellent local control was achieved, an unexpectedly higher enucleation rate was obtained owing to newly developed neovascular glaucoma, which was the most serious anterior segment complication [4].

Although a simple shell alone was used for linac-based small-field radiotherapy with fractionated SRT [23, 24], it was of utmost importance to overcome the technical challenge of immobilization of the affected eye in the appropriate position during the fractionated external beam therapy [7]. Various immobilization techniques for the affected eye have been reported [4, 8–15]. One such accurate fixation system is an invasive suction fixation method for radiosurgery for intraocular melanoma using retrobulbar anesthesia [25]. In proton beam therapy and when SRT was first introduced, patients were asked to focus on a light, while the gaze direction of the eye was checked by the position of radiopaque clips or tantalum rings sutured in the sclera on a film before treatment [4, 26–28]. The advanced method involved voluntary fixation of the eye throughout the procedure by monitoring the eye using a CCD camera and television system [8–15].

We developed a non-invasive method using an optic F-M device during treatment planning. The whole treatment procedure was conducted with the prism mirror attached to the immobilization shell to ensure that the optic axis was maintained in the correct position with respect to the gazing light on the side of the camera. The

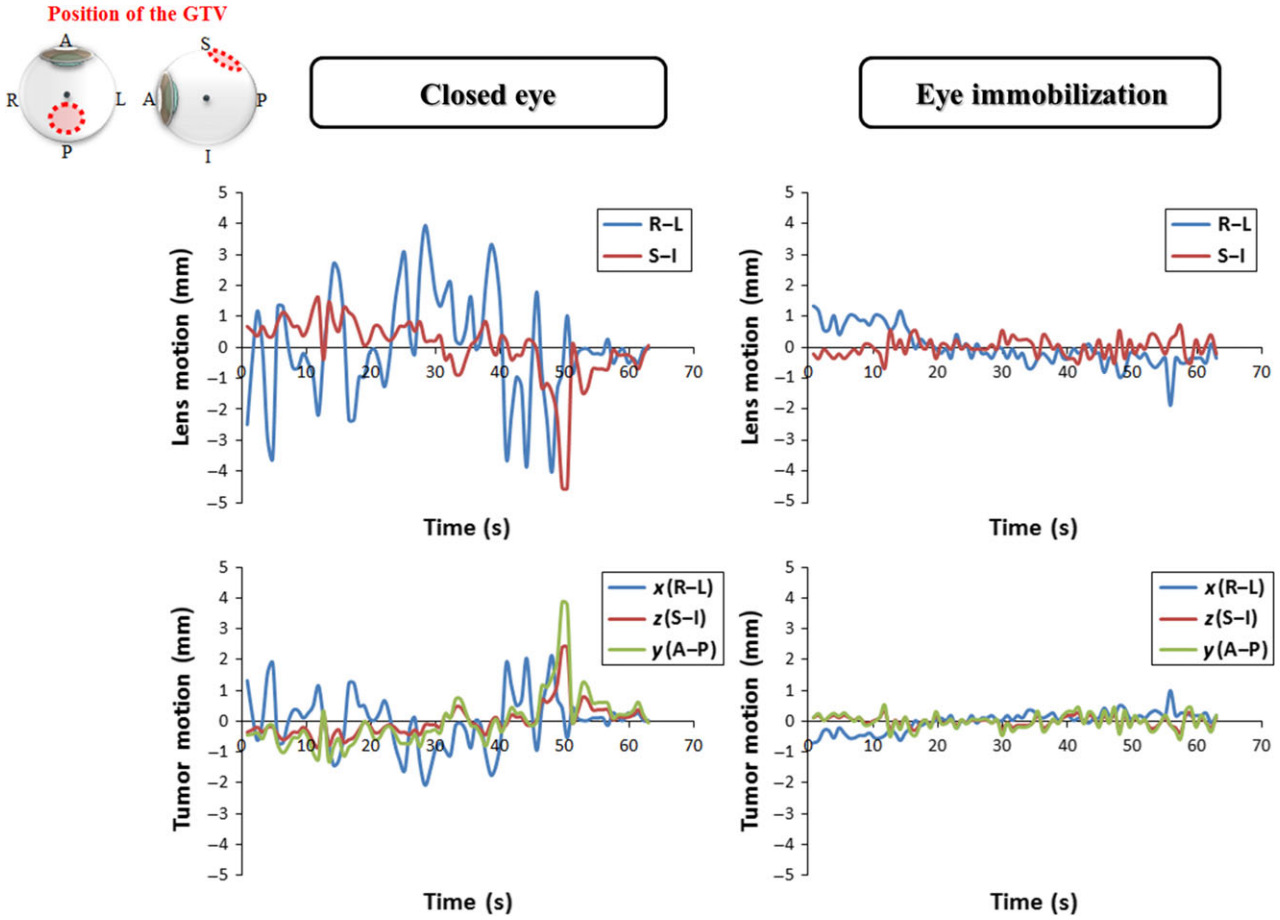

Fig. 6. Relationship between lens movement and tumor position (an example of calculated tumor motion). The upper figure shows lens motion, and the lower figure shows calculated tumor motion. The left figure was obtained using the immobilization shell with closed eyes; the right figure was obtained using the immobilizing shell with opened eyes.

consequences of eye movements with regard to the accuracy of tumor irradiation were calculated in the study by Muller *et al.* [7]. They reported that an eye rotation of 12° would result in a shift of 2 mm when the mean distance between the center of the eye and the center of the GTV was 9.5 mm. Their study included 2 (of 19) patients who had rotations larger than 12°. Since our method involved using a prism mirror to align the optic axis connecting the cornea and pupil centers with the gazing direction of the antero–posterior axis, we could eliminate the shift resulting from the rotation of the eye. Repositioning accuracy was improved owing to repeated determination of the position of the GTV at every IMRT session.

George *et al.* [13] evaluated the impact of a micro-multileaf collimator (mMLC) on SRT for uveal melanoma by comparing circular arc with static conformal, dynamic arc, and intensity-modulated SRT. They concluded that conformal mMLC and dynamic arc SRT is the treatment of choice. On the other hand, IMRT was not recommended because of the larger number of MUs necessary to deliver the prescribed dose, which resulted in an increase in delivery time. However, the actual beam-on time was ~45 s per beam in our study; therefore, the patients could tolerate the in-house F-M device method well. In addition, they found that IMRT was not remarkably advantageous in terms of optical nerve sparing, but it was advantageous in terms of lens sparing. Regarding SRT for choroidal melanoma of the posterior arcade of the retina, the most challenging issue remaining concerns how to decrease the dose to the fovea and the disc. In fact, for the three patients discussed herein, the tumor was located at the posterior arcade of the retina. In this study, we analyzed the lens motion using Cine MRI, and we calculated the coordinate rotation based on the lens motion in order to predict the IM of the tumor on the choroid from the movements of the eyeball. The in-house F-M device enabled a decrease in the voluntary movement of the eyeballs; therefore, the PTV decreased and the DVH parameters for the PTV, GTV, fovea, disc, optic nerve, retina, eyeball, lens, and lachrymal gland improved (Table 3). We decreased the dose to the fovea and the disc from 75 to 17% and from 46 to 14%, respectively in Patient #1. Consistently, her visual acuity did not decrease 25 months after treatment.

Dieckmann reported that the mean relative reductions in tumor size were 24%, 27% and 37% after 12, 24 and 36 months, respectively [29]. Patient #1 showed satisfactory tumor regression on the follow-up CT images. Concerning adverse effects, she only

Table 3. DVH parameter with and without the F-M device

Patient #		#1		#2		#3	
F-M device		(−)	(+)	(−)	(+)	(−)	(+)
Object		Dose (%)	Dose (%)	Dose (%)	Dose (%)	Dose (%)	Dose (%)
PTV	D_{95}	97.1	97.2	97.3	97.3	98.9	98.9
	V_{107}	3.6	3.6	0.0	0.0	0.0	0.0
	D_{98}	94.6	95.3	96.2	95.6	97.8	97.9
	D_{50}	104.5	103.6	101.1	102.0	102.4	103.3
	D_{2}	107.5	108.3	103.9	103.9	104.0	105.7
GTV	D_{99}	103.8	103.1	101.2	101.2	102.0	102.0
	D_{50}	105.3	105.3	102.8	102.8	103.3	104.3
Fovea (point dose)		103.5	43.0	96.5	94.5	35.5	29.4
Disc (point dose)		45.7	13.7	92.9	87.5	39.8	29.1
Optic nerve	D_{max}	87.7	53.6	98.3	94.6	72.3	57.4
	$D_{0.1\ cm^3}$	21.0	5.8	36.5	31.6	30.7	23.5
	D_{mean}	7.2	2.7	14.5	12.0	13.1	9.8
Retina	D_{max}	108.6	111.7	103.7	104.0	105.0	105.6
	$D_{0.1\ cm^3}$	106.1	105.3	98.9	98.7	102.9	102.7
	$D_{0.5\ cm^3}$	99.7	79.9	39.9	34.9	43.5	35.8
	$D_{1\ cm^3}$	57.9	41.6	4.3	2.9	1.8	1.1
	D_{mean}	33.2	25.6	28.4	26.0	39.9	34.9
Eyeball	D_{max}	108.1	111.7	104.4	104.2	105.0	105.7
	$D_{1\ cm^3}$	96.3	74.6	76.7	66.1	96.1	85.9
	$D_{5\ cm^3}$	15.1	6.4	2.0	1.6	16.6	11.3
	D_{mean}	33.1	24.1	22.7	19.9	35.8	29.9
Lens	D_{max}	23.4	17.2	0.8	0.7	29.2	21.6
	$D_{0.1\ cm^3}$	2.8	1.4	0.3	0.3	11.2	5.4
	D_{mean}	5.1	2.2	0.5	0.5	12.8	8.2
Lacrimal gland	D_{max}	106.8	103.9	35.1	30.5	26.1	22.7
	$D_{0.1\ cm^3}$	99.2	82.4	9.8	7.0	12.6	9.0
	$D_{0.5\ cm^3}$	13.1	4.9	0.9	0.8	0.8	0.6
	D_{mean}	63.0	48.8	3.0	2.3	4.5	3.4

DVH = dose–volume histogram; F-M device = fixation and monitoring device; PTV = planning target volume; GTV = gross tumor volume.

developed low-grade cataract without dry eye syndrome, which was related to the dose distribution to the lacrimal gland [30].

In recent years, Daftari *et al.* [31] pointed out that particle beam irradiation to the anterior segment was highly correlated with the development of neovascular glaucoma, and they described an approach using the CyberKnife for extra-large choroidal or cilio-choroidal melanomas. They reported a long treatment time using the CyberKnife: in non-isocentric irradiation with CyberKnife, the

Table 4. MUs and treatment duration

Patient #	#1	#2	#3
PTV (mm^3)	1028	395	753
Dose (Gy)/fractions	60/5	60/5	60/5
# Beams	7	7	7
MUs required to deliver 12 Gy —per one of seven beams	359 (279–416)	329 (294–340)	310 (82–344)
Treatment duration (min) —including set-up	28.3 (24.5–34.3)	25.7 (20.4–36.4)	48.4 (27.3–82.6)
Beam-on time (sec) —to deliver dose/beams	43 (35–52)	41 (37–43)	39 (35–43)

PTV = planning target volume; MUs = monitor units.

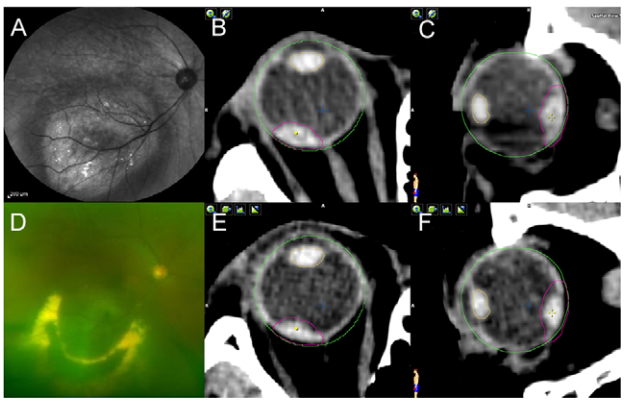

Fig. 7. In Patient #1, the tumor was located at the inferior temporal arcade of the right retina. Distances to the fovea and disc were estimated at 5.3 mm and 9.6 mm, respectively. The gross tumor volume was 12.8 × 10.0 × 5.7 mm (A, B, C). After 25 months, this decreased in size to 11.4 × 9.1 × 5.0 mm and demonstrated hard exudates at the tumor margin upon fundoscopy (D, E, F).

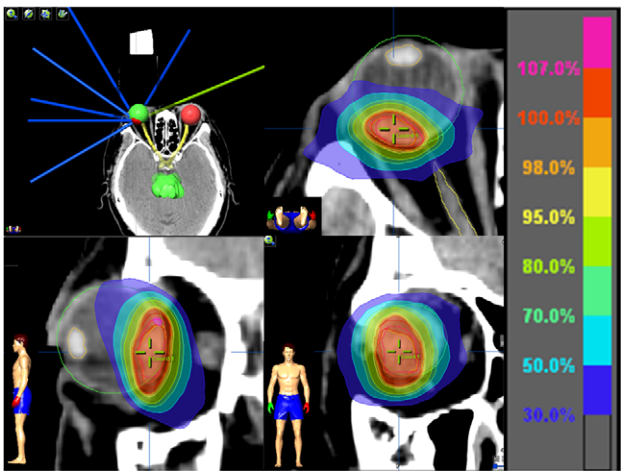

Fig. 8. Patient #1 underwent curative intensity-modulated radiotherapy comprising 60 Gy administered in five fractions over 7 days using seven non-coplanar beams.

irradiation time is extended by a large PTV size. In our research, we have adapted the versatile type of linac-based machine. Therefore, variation in PTV size has little impact on treatment time. There are other reports of systems involving advanced mechanisms, such as OCT or tracking systems. They have higher prediction accuracy regarding tumor location [32, 33]; however, these systems require expensive special materials. For predicting tumor position and for reducing the dose to the anterior segment, our study is adequate for clinical use. In addition, this method is capable of adoption in any institute at a low cost.

In our clinical experience, which involves a limited number of patients, our simple in-house F-M device system for immobilizing eyeballs was well tolerated by all three consecutive IMRT patients with choroidal melanoma. Since the classic tolerance dose proposed for the retina in conventional fractionated radiotherapy does not apply to the modern IMRT technology and fractionation for choroidal melanoma [34, 35], up-to-date information is necessary for determining the relevant tolerance dose for future IMRT strategies involving the F-M device. Therefore, additional cases and accumulation of precise treatment data is necessary.

CONCLUSION

We developed a non-invasive F-M device for immobilizing eyeballs during the treatment planning and IMRT for choroidal melanoma (using a prism mirror mounted on the immobilization shell to ensure that the optic axis is in the correct position with respect to the gazing light on the side of the camera). We analyzed the lens motion (which predicted the IM of the choroidal tumor) from movements of the eyeball using Cine MRI. Using these methods,

we could accurately determine the position of the GTV each day. Owing to the reduced PTV, doses to OARs were markedly reduced. Although the treatment duration was longer in some sessions, the beam-on time was short for all patients. Therefore, all patients tolerated this method well. The results of this study demonstrate the feasibility and efficacy of our in-house F-M device for immobilizing eyeballs during IMRT for choroidal melanoma.

ACKNOWLEDGEMENTS

We sincerely thank Nathalie Fournier-Bidoz, PhD, Institut Curie, for her useful comments on this paper. We would like to thank Editage (www.editage.jp) for English language editing.

CONFLICT OF INTEREST

The authors report that there are no conflicts of interest.

REFERENCES

1. Center for Cancer Control and Information Services, National Cancer Center. Report of rare cancer work-shop (20 March 2014, in Japanese). http://www.ncc.go.jp/jp/cis/divisions/06health_s/files/06health_s_work.pdf (17 January 2016, date last accessed).
2. Al-Wassia R, Dal Pra A, Shun K, et al. Stereotactic fractionated radiotherapy in the treatment of juxtapapillary choroidal melanoma: the McGill University experience. *Int J Radiat Oncol Biol Phys* 2011;81:e455–62.
3. Muller K, Naus N, Nowak PJ, et al. Fractionated stereotactic radiotherapy for uveal melanoma, late clinical results. *Radiother Oncol* 2012;102:219–24.
4. Gragoudas ES. Proton beam irradiation of uveal melanomas: the first 30 years. The Weisenfeld Lecture. *Invest Ophthalmol Vis Sci* 2006;47:4666–73.
5. Okada T, Kamada T, Tsuji H, et al. Carbon ion radiotherapy: clinical experiences at National Institute of Radiological Science (NIRS). *J Radiat Res* 2010;51:355–64.
6. Tsuji H, Ishikawa H, Yanagi T, et al. Carbon-ion radiotherapy for locally advanced or unfavorably located choroidal melanoma: a phase I/II dose escalation study. *Int J Radiat Oncol Biol Phys* 2007;67:857–62.
7. Muller K, Nowak PJ, Luyten GP, et al. A modified relocatable stereotactic frame for irradiation of eye melanoma: design and evaluation of treatment accuracy. *Int J Radiat Oncol Biol Phys* 2004;58:284–91.
8. Dieckmann K, Bogner J, Georg D, et al. A linac-based stereotactic irradiation technique of uveal melanoma. *Radiother Oncol* 2001;61:49–56.
9. Buchgeister M, Grisanti S, Süsskind D, et al. A new fixation aid for the radiotherapy of eye tumors. *Med Phys* 2007;34:4649–53.
10. Bogner J, Petersch B, Georg D, et al. A noninvasive eye fixation and computer-aided eye monitoring system for linear accelerator–based stereotactic radiotherapy of uveal melanoma. *Int J Radiat Oncol Biol Phys* 2003;56:1128–36.
11. Petersch B, Bogner J, Dieckmann K, et al. Automatic real-time surveillance of eye position and gating for stereotactic radiotherapy of uveal melanoma. *Med Phys* 2004; 31:3521–7.
12. Shin D, Yoo SH, Moon SH, et al. Eye tracking and gating system for proton therapy of orbital tumors. *Med Phys* 2012;39: 4265–73.
13. Georg D, Dieckmann K, Bogner J, et al. Impact of a micromutileaf collimator on stereotactic radiotherapy of uveal melanoma. *Int J Radiat Oncol Biol Phys* 2003;55:881–91.
14. Fassi A, Riboldi M, Forlani CF, et al. Optical eye tracking system for noninvasive and automatic monitoring of eye position and movements in radiotherapy treatments of ocular tumors. *Appl Opt* 2012;51:2441–50.
15. Jaywant SM, Osei EK, Ladak S. Stereotactic radiotherapy in the treatment of ocular melanoma: a noninvasive eye fixation aid and tracking system. *J Appl Clin Med Phys* 2003;4:156–61.
16. Inoue T, Masai N, Oh RJ, et al. Adaptive replanning intensity-modulated radiotherapy for choroidal metastasis of breast cancer using optical coherence tomography. *J Radiat Res* 2014;55:502–8.
17. Metz HS, Salazar OM, Rubin P. Tumors of the eye. In: Rubin P, ed. *Clinical Oncology for Medical Students and Physicians. Multidisciplinary Approach*. 6th edn. Atlanta: American Cancer Society, Inc. 1983, 280–94.
18. Gragoudas, ES, Goitein M, Verhey MR, et al. Proton beam irradiation. An alternative to enucleation for intraocular melanomas. *Ophthalmology* 1980;87:571–81.
19. Packer S, Rotman M, Fairchild RG, et al. Irradiation of choroidal melanoma with iodine-125 ophthalmic plaque. *Arch Ophthalmol* 1980;98:1453–7.
20. Char DH, Castro JR, Quivey JA, et al. Helium ion charged particle therapy for choroidal melanoma. *Arch Ophthalmol* 1980; 87:565–70.
21. Marchini G, Gerosa M, Piovan E, et al. Gamma Knife stereotactic radiosurgery for uveal melanoma: clinical results after 2 years. *Stereotact Funct Neurosurg* 1996;66:208–13.
22. Strauss A, Dritschilo A, Nathanson L, et al. Radiation therapy of malignant melanomas: an evaluation of clinically used fractionation schemes. *Cancer* 1981;47:1252–6.
23. Tokuuye K, Akine Y, Tokita N, et al. Linac-based small-field radiotherapy for brain tumors. *Radiother Oncol* 1993;27:55–8.
24. Tokuuye K, Sumi M, Kagami Y, et al. Long-term observations of a patient with choroidal melanoma following fractionated stereotactic radiotherapy: a case report. *Acta Ophthalmol Scand* 2000;78:477–9.
25. Zehetmayer M, Menapace R, Kitz K, et al. Experience with a suction fixation system for stereotactic radiosurgery of intraocular malignancies. *Stereotact Funct Neurosurg* 1995;64: 80–6.
26. Zehetmayer M, Schima W, Menapace R, et al. Radio-opaque markers for stereotactic imaging of uveal melanoma. *Br J Radiol* 1998;71:630–3.
27. Egger E, Schalenbourg A, Zografos L, et al. Maximizing local tumor control and survival after proton beam radiotherapy of uveal melanoma. *Int J Radiat Oncol Biol Phys* 2001;51: 138–47.
28. Fuss M, Loredo LN, Blacharski PA, et al. Proton radiation therapy for medium and large choroidal melanoma: preservation of the eye and its functionality. *Int J Radiat Oncol Biol Phys* 2001; 49:1053–9.

29. Dieckmann K, Georg D, Zehetmayer M, et al. LINAC based stereotactic radiotherapy of uveal melanoma: 4 years clinical experience. *Radiother Oncol* 2003;67:199–206.
30. Muller K, Nowak PJ, Naus N, et al. Lacrimal gland radiosensitivity in uveal melanoma patients. *Int J Radiat Oncol Biol Phys* 2009;74:497–502.
31. Daftari IK, Petti PL, Larson DA, et al. A noninvasive eye fixation monitoring system for CyberKnife radiotherapy of choroidal and orbital tumors. *Med Phys* 2009;36:719–24.
32. Rüegsegger MB, Geiser D, Steiner P, et al. Noninvasive referencing of intraocular tumors for external beam radiation therapy using optical coherence tomography: a proof of concept. *Med Phys* 2014;41:081704.
33. Via R, Fassi A, Fattori G, et al. Optical eye tracking system for real-time noninvasive tumor localization in external beam radiotherapy. *Med Phys* 2015;42:2194–202.
34. Emami B, Lyman J, Brown A, et al. Tolerance of normal tissue to therapeutic irradiation. *Int J Radiat Oncol Biol Phys* 1991;15:109–22.
35. Marks LB, Yorke ED, Jackson A, et al. Use of normal tissue complication probability models in the clinic. *Int J Radiat Oncol Biol Phys* 2010;76:S10–S19.